Rock Mech. Rock Engng. (2004) 37 (2), 127–150
DOI 10.1007/s00603-003-0023-y

Rock Mechanics and Rock Engineering
Printed in Austria

Analysis of Wedge Stability Using Different Methods

By

Y.-J. Wang[1], **J.-H. Yin**[2], **Z. Chen**[3], and **C. F. Lee**[4]

[1] China Institute of Water Resources and Hydraulic Power Research, Beijing, P.R. China
[2] Department of Civil and Structural Engineering, The Hong Kong Polytechnic University, Hong Kong, P.R. China
[3] China Institute of Water Resources and Hydraulic Power Research, Beijing, P.R. China
[4] Department of Civil Engineering, The University of Hong Kong, Hong Kong, P.R. China

Received September 8, 2002; accepted August 29, 2003
Published online February 18, 2004 © Springer-Verlag 2004

Summary

The stability problem of a rock slope containing a wedge resting on two intersecting discontinuities is of great interest in rock slope engineering. It is a statistically indeterminate problem with two extra unknowns according to the force (stress) equilibrium analysis. The widely used limit equilibrium methods in practice assume that the directions of the shear forces acting on the two discontinuities are parallel to their line of intersection. The validity of this assumption, however, has not been verified theoretically. This paper presents a general limit equilibrium method that determines the directions of the shear forces by using Pan's ''Maximum principle'' and an upper bound method that applies the classic upper bound theorem of limit analysis to avoid making extra assumptions. The formulations of the two methods are derived. A non-symmetric wedge and a symmetric wedge are analyzed using the two derived methods. To further explore the influence on stability due to the direction of the shear force acting on the two discontinuities, three-dimensional finite-element analyses are also conducted. The results are compared and discussed.

Keywords: Wedge, dilatancy, stability, factor of safety, upper bound, finite element method.

List of Symbols

A_1, A_2	areas of plane
c, c_1, c_2	cohesions of the soil
c_{e1}, c_{e2}	mobilized cohesions
$\boldsymbol{D}$	energy dissipation along shear band
E_{slip}	elasticity modulus of the material for the slip zone
E_{wedge}	elasticity modulus of the wedge body

F	factor of safety
$\boldsymbol{G}$	weight of the wedge
n	the number of nodes on a plane
$\boldsymbol{n}_1$, $\boldsymbol{n}_2$	unity norm vectors
n_{1x}, n_{1y}, n_{1z}	the components of $\boldsymbol{n}_1$ in (x, y, z) coordinate system
n_{2x}, n_{2y}, n_{2z}	the components of $\boldsymbol{n}_2$ in (x, y, z) coordinate system
$\boldsymbol{P}$	resultant force of pore water pressure
$\boldsymbol{P}_1$, $\boldsymbol{P}_2$	uplift forces
r_{xi}, r_{yi}, r_{zi}	the components of reaction $\boldsymbol{R}$ of node i in x, y and z directions
$\boldsymbol{R}$, $\boldsymbol{R}_1$, $\boldsymbol{R}_2$	reactions acted on the plane
$\boldsymbol{R}_{1n}$, $\boldsymbol{R}_{1s}$	the components of $\boldsymbol{R}_1$
$\boldsymbol{R}_{2n}$, $\boldsymbol{R}_{2s}$	the components of $\boldsymbol{R}_2$
$\boldsymbol{S}_1$	shear force
$\boldsymbol{S}_{11}$, $\boldsymbol{S}_{22}$	forces parallel to the line of intersection
$\boldsymbol{T}$	external surface load
$\boldsymbol{T}_r$	the resultant of forces $\boldsymbol{G}$, $\boldsymbol{T}$, $\boldsymbol{P}_1$ and $\boldsymbol{P}_2$
$\boldsymbol{T}_{rs}$, $\boldsymbol{T}_{rn}$	the components of $\boldsymbol{T}_r$ along and perpendicular to the line of intersection
$\boldsymbol{T}^*$	external surface load over the velocity field $\boldsymbol{V}^*$
v_x, v_y, v_z	the components of velocity jump $\boldsymbol{V}$ in (x, y, z) coordinate system
$\boldsymbol{V}$	velocity jump
$\lvert\boldsymbol{V}\rvert$	the magnitude of $\boldsymbol{V}$
$\boldsymbol{V}^*$	velocity field
α, α_1, α_2	angles between the intersection line and the direction of force $\boldsymbol{T}_r$
β_1, β_2	inclination angles of $\boldsymbol{S}_1$ and $\boldsymbol{S}_2$ to the intersection line
γ_{slip}	unit weight of the material for the slip zone
γ_{wedge}	unit weight of the wedge body
ν_{wedge}	Poisson's ratio of the wedge body
θ_1, θ_2	the inclinations of $\boldsymbol{R}_1$ and $\boldsymbol{R}_2$ with respect to the direction of $\boldsymbol{T}_{rn}$
σ_{ij}^*, $\dot{\varepsilon}_{ij}^*$	stress and strain rate within plastic zone Ω^*
σ_{Γ^*}, $\dot{\varepsilon}_{\Gamma^*}$	stress and strain rate over slip surface Γ^*.
ϕ, ϕ_1, ϕ_2	friction angles of the soil
ϕ_{e1}, ϕ_{e2}	mobilized friction angles
ψ_e	dilation angle of the soil
κ, κ_1, κ_2	yielding ratios
$\Phi(\boldsymbol{V} \bullet \boldsymbol{n}_i)$	scalar product of vectors $\boldsymbol{V}$ and $\boldsymbol{n}_i$, $i = 1,2$
Γ^*	slip surface
Ω^*	plastic zone

1. Introduction

Stability analysis of a rock slope containing a wedge resting on two interesting discontinuities is of great interest in rock slope engineering. A spatial force equilibrium analysis shows that the problem of wedge stability is statistically indeterminate with two extra unknowns (Wang and Yin, 2002). To render this problem resolvable, traditional limit equilibrium methods assume that the directions of the shear forces applied on the two intersecting discontinuities are parallel to the line of intersection of these two discontinuities (Hoek et al., 1973; Goodman, 1995). However, the validity of this assumption has not been verified. By considering dilatancy properties of discontinuities during shearing and using the limit equilibrium approach, Wang and Yin (2002) found that the directions of the shear forces acting on these two intersecting discontinuities incline a certain angle to the line of intersection when the dilation angles associated with the discontinuities vary. This means that the results of stability analysis of the wedge problem depend on the assumptions regarding the directions of the shear forces acting along the discontinuities.

Focusing on slope stability analysis, Pan (1980) suggested that for a specified slip surface, the stresses within the failing rock volume as well as on the slip surface will be readjusted to mobilize the maximum resistance against failure. This idea might provide a way for determining the directions of the shear forces that mobilize the maximum resistance. In addition, by establishing a work-energy-balance equation, the widely used upper-bound method of limit analysis in geotechnical engineering (Chen, 1975; Michalowski, 1995) allows one to find the factor of safety by solving this equation. Application of the upper bound method, therefore, could provide another way of solving the wedge problem without making assumptions regarding the shear forces directions. With the advances in computer technology, the finite element (FE) method has become a powerful tool for numerical solution of a wide range of geotechnical engineering problems (Desai et al., 1984), and a three-dimensional (3-D) finite element analysis may throughout explore the wedge problem.

The objectives of the paper are: (a) to derive a general formulation for the wedge stability analysis based on the limit equilibrium approach without any additional assumption; (b) to derive a particular equation of a general limit equilibrium method based on Pan's ''Maximum Principle''; (c) to derive the formulation of an upper bound method for the wedge stability analysis; (d) to analyze the problem of wedge stability by using a 3-D FE model; and (e) to explore the influence of the directions of the shear forces acting on the discontinuities on the factor of safety by using the finite element method.

2. General Equations for Calculation of the Factor of Safety

In the following stability analyses of the wedge problems, the two intersecting discontinuities, on which a wedge rests, are assumed to be through-going and planar. The left discontinuity is called plane A while the right one is called plane B (Fig. 1). The wedge is subjected to an external surface load $\boldsymbol{T}$, weight of the wedge $\boldsymbol{G}$, uplift force $\boldsymbol{P}_1$ acting on plane A and uplift force $\boldsymbol{P}_2$ acting on plane B. For convenience, the resultant of forces $\boldsymbol{G}$, $\boldsymbol{T}$, $\boldsymbol{P}_1$ and $\boldsymbol{P}_2$ is defined as a force $\boldsymbol{T}_r$.

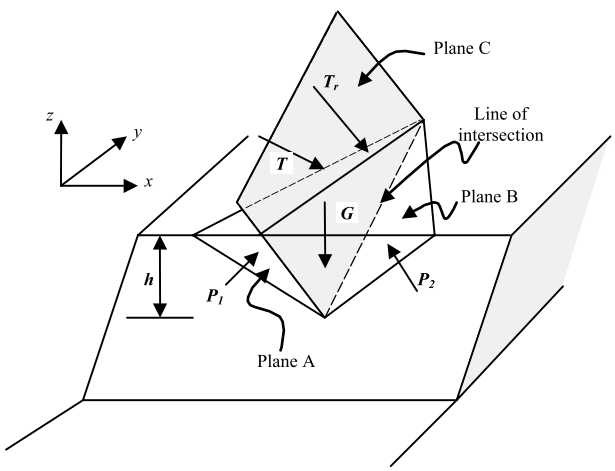

Fig. 1. An isometric view of a slope containing a wedge and forces applied on it

The plane passing through $\boldsymbol{T_r}$ and the line of intersection of planes A and B is defined as plane C. If the direction of $\boldsymbol{T_r}$ is downwards and lies between planes A and B, the wedge would slide along these two intersecting discontinuities, which is the case to be analyzed in this paper. However, when the direction of $\boldsymbol{T_r}$ is downwards and not between planes A and B, the wedge would fail along one of these two discontinuities. It is a typical slope stability problem with one slip surface, which is not considered in this paper.

When considering a potential sliding of the wedge along the line of intersection of two interesting discontinuities, a unique decomposition of force $\boldsymbol{T_r}$ on plane C into a component $\boldsymbol{T_{rs}}$ along the line of intersection and a component $\boldsymbol{T_{rn}}$ perpendicular to the line of intersection can be written as follows (Fig. 2a):

$$T_{rs} = T_r \cdot \cos\alpha, \tag{1}$$

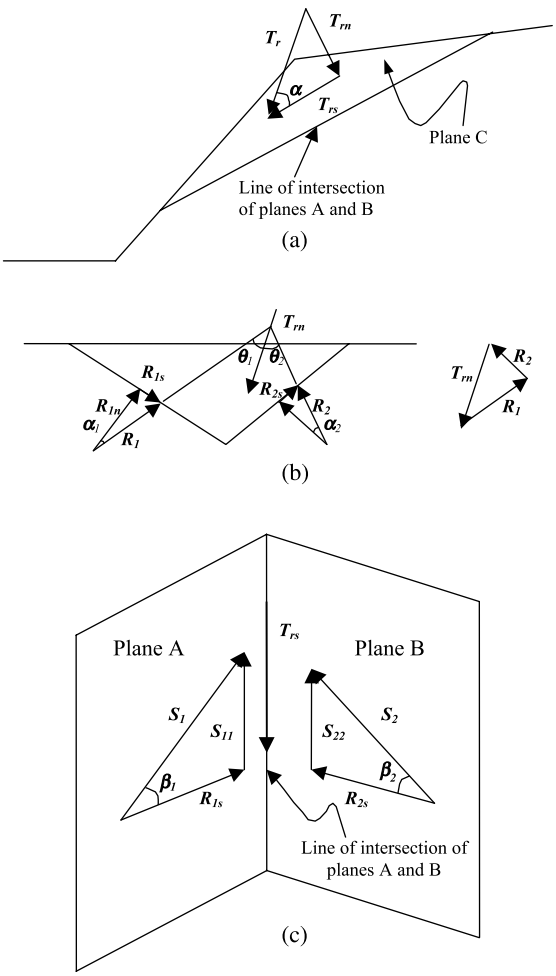

Fig. 2. Forces applied on the wedge and their decompositions. **a**) plane passing through force $\boldsymbol{T_r}$ and the line of intersection of planes A and B; **b**) plane normal to the line of intersection of planes A and B; **c**) aerial view of planes A and B

$$T_{rn} = T_r \cdot \sin\alpha, \tag{2}$$

where α is the angle between the line of intersection of planes A and B and the direction of force $\boldsymbol{T_r}$.

Since it is not necessary to require reactions of planes A and B to $\boldsymbol{T_{rn}}$ to be normal to these two planes, the resolution of $\boldsymbol{T_{rn}}$ into two components acting on planes A and B is indefinite. The reactions $\boldsymbol{R}_1$ and $\boldsymbol{R}_2$ of planes A and B to force $\boldsymbol{T_{rn}}$ have infinite sets of combinations as shown in Fig. 2b. They respectively incline at θ_1 and θ_2 with respect to the direction of force $\boldsymbol{T_{rn}}$. The angles θ_1 and θ_2 may have indefinite sets. The case that reactions $\boldsymbol{R}_1$ and $\boldsymbol{R}_2$ are normal to planes A and B is a special one and is commonly adopted in traditional limit equilibrium methods (Hoek et al., 1973).

A force-triangle analysis of $\boldsymbol{R}_1$, $\boldsymbol{R}_2$ and $\boldsymbol{T_{rn}}$ yields

$$R_1 = \frac{\sin\theta_2}{\sin(\theta_1+\theta_2)} \cdot T_{rn} = \frac{\sin\theta_2}{\sin(\theta_1+\theta_2)} \cdot \sin\alpha \cdot T_r, \tag{3}$$

$$R_2 = \frac{\sin\theta_1}{\sin(\theta_1+\theta_2)} \cdot T_{rn} = \frac{\sin\theta_1}{\sin(\theta_1+\theta_2)} \cdot \sin\alpha \cdot T_r, \tag{4}$$

in which $\boldsymbol{R}_1$ and $\boldsymbol{R}_2$ incline at angles α_1 and α_2 with respect to normals to planes A and B respectively (Fig. 2b). By focusing on forces acting on plane A, $\boldsymbol{R}_1$ is resolved into two components $\boldsymbol{R_{1n}}$ and $\boldsymbol{R_{1s}}$ on a plane perpendicular to the line of intersection of planes A and B. As illustrated in Fig. 2(b), $\boldsymbol{R_{1n}}$ is normal to plane A and $\boldsymbol{R_{1s}}$ is along the line of intersection of plane A and a plane perpendicular to the line of intersection of planes A and B. Thus,

$$R_{1n} = R_1 \cdot \cos\alpha_1, \tag{5}$$

$$R_{1s} = R_1 \cdot \sin\alpha_1. \tag{6}$$

Since all forces on the plane perpendicular to the line of intersection of planes A and B are in equilibrium, force equilibrium analysis shows that a force $\boldsymbol{S}_{11}$ that is parallel to the line of intersection of planes A and B should exist to resist force $\boldsymbol{T_{rs}}$ (Fig. 2c). The resultant force of $\boldsymbol{S}_{11}$ and $\boldsymbol{R_{1s}}$ constitutes a shear force $\boldsymbol{S}_1$ acting on plane A, which is related to force $\boldsymbol{R_{1n}}$ by the Mohr-Coulomb failure criterion (Fig. 2c)

$$S_1^2 = S_{11}^2 + R_{1s}^2 = (R_{1n} \cdot \tan\phi_{e1} + c_{e1} \cdot A_1)^2, \tag{7}$$

where c_{e1} and ϕ_{e1} are the mobilized cohesion and angle of internal friction associated with plane A, respectively. A_1 is the area of plane A. c_{e1} and ϕ_{e1} are related to the factor of safety F by $F = \frac{\tan\phi_1}{\tan\phi_{e1}} = \frac{c_1}{c_{e1}}$, in which c_1 and ϕ_1 are the cohesion and angle of internal friction associated with plane A, respectively. Force $\boldsymbol{S}_1$ inclines at an angle β_1 to the line of intersection of planes A and B (Fig. 2c). Substitution of Eqs. (3), (5) and (6) into Eq. (7) and rearranging yields

$$S_{11} = \sqrt{\begin{array}{l}\frac{\sin^2\theta_2}{\sin^2(\theta_1+\theta_2)} \cdot \sin^2\alpha \cdot T_r^2 \cdot [\cos^2\alpha_1 \tan^2\phi_{e1} - \sin^2\alpha_1] + \\ +2c_{e1} \cdot A_1 \cdot \tan\phi_{e1} \cdot \frac{\sin\theta_2}{\sin(\theta_1+\theta_2)} \cdot \sin\alpha \cdot \cos\alpha_1 \cdot T_r + c_{e1}^2 \cdot A_1^2 \cdot\end{array}} \tag{8}$$

Similarly, a force $\boldsymbol{S}_{22}$ on plane B that is parallel to the line of intersection of planes A and B to resist $\boldsymbol{T}_{rs}$ is

$$S_{22} = \sqrt{\begin{array}{l}\frac{\sin^2\theta_1}{\sin^2(\theta_1+\theta_2)} \cdot \sin^2\alpha \cdot T_r^2 \cdot [\cos^2\alpha_2 \tan^2\phi_{e2} - \sin^2\alpha_2] + \\ +2c_{e2} \cdot A_2 \cdot \tan\phi_{e2} \cdot \frac{\sin\theta_1}{\sin(\theta_1+\theta_2)} \cdot \sin\alpha \cdot \cos\alpha_2 \cdot T_r + c_{e2}^2 \cdot A_2^2\end{array}} \tag{9}$$

where c_{e2} and ϕ_{e2} are moblized cohesion and angle of internal friction associated with plane B, respectively. A_2 is the area of plane B.

Establishing the force equilibrium equation along the line of intersection of planes A and B yields

$$S_{11} + S_{22} = T_{rs}. \tag{10}$$

Substituting Eqs. (1), (8) and (9) into Eq. (10) and after rearranging gives

$$\begin{array}{l}\sqrt{\begin{array}{l}\frac{\sin^2\theta_2}{\sin^2(\theta_1+\theta_2)} \cdot \tan^2\alpha \cdot (\cos^2\alpha_1 \tan^2\phi_{e1} - \sin^2\alpha_1) + \\ +2c_{e1} \cdot A_1 \cdot \tan\phi_{e1} \cdot \frac{\sin\theta_2}{\sin(\theta_1+\theta_2)} \cdot \cos\alpha_1 \cdot \frac{\tan\alpha}{\cos\alpha \cdot T_r} + \frac{c_{e1}^2 \cdot A_1^2}{\cos^2\alpha \cdot T_r^2}\end{array}} \\ + \sqrt{\begin{array}{l}\frac{\sin^2\theta_1}{\sin^2(\theta_1+\theta_2)} \cdot \tan^2\alpha \cdot (\cos^2\alpha_2 \tan^2\phi_{e2} - \sin^2\alpha_2) + \\ +2c_{e2} \cdot A_2 \cdot \tan\phi_{e2} \cdot \frac{\sin\theta_1}{\sin(\theta_1+\theta_2)} \cdot \cos\alpha_2 \cdot \frac{\tan\alpha}{\cos\alpha \cdot T_r} + \frac{c_{e2}^2 \cdot A_2^2}{\cos^2\alpha \cdot T_r^2}\end{array}} = 1.\end{array} \tag{11}$$

Note that when the wedge geometry, the external loading condition and strength parameters associated with the two discontinuities are specified, there are three unknowns F, θ_1 and θ_2 involved in Eq. (11). One equation with three unknowns obviously indicates that the wedge stability is a statistically indeterminate problem and the factor of safety cannot be determined by Eq. (11) without introducing any extra assumption (such as directions of shear forces).

3. Traditional Limit Equilibrium Method (TLE)

In traditional limit equilibrium methods it is generally assumed that shear forces $\boldsymbol{S}_1$ and $\boldsymbol{S}_2$ acting on planes A and B are parallel to the line of intersection of the two planes. It means that forces $\boldsymbol{R}_{1s}$ and $\boldsymbol{R}_{2s}$ diminish and reactions of discontinuities to force $\boldsymbol{T}_{rn}$ are in directions of normals to planes A and B ($\alpha_1 = \alpha_2 = 0$). After rearranging Eq. (11), the factor of safety F for the **TLE** method is rewritten as

$$F = \frac{\tan a}{\sin(\theta_1+\theta_2)}(\sin\theta_2 \tan\phi_1 + \sin\theta_1 \tan\phi_2) + \frac{(c_1A_1 + c_2A_2)}{T_r \cos\alpha}. \tag{12}$$

Since forces $\boldsymbol{R}_{1s}$ and $\boldsymbol{R}_{2s}$ are in directions of normals to planes A and B, when the external force $\boldsymbol{T}_r$ is known, angles θ_1 and θ_2 are uniquely determined and the factor of safety F can be obtained explicitly using Eq. (12).

4. General Limit Equilibrium (GLE) Method

When directions of shear forces acting on planes A and B are not assumed to be parallel to the line of intersection of these two planes, it is crucial to provide two extra equations to make the wedge problem statically determinate. Two postulates for slope stability analysis proposed by Pan (1980) allow one to solve this problem. They are: (a) Among many possible slip surfaces, the real one offers the minimum resistance against failure, which is called ''Principle of Minimum''; (b) For a specified slip surface, the stress within the failing mass as well as on the slip surface will be readjusted to mobilize the maximum resistance against failure, which is called ''Principle of Maximum''.

These two postulates propose a general and abstractive way of performing slope stability analyses. They are applicable to all slope stability problems. The slip surface may be two-dimensional (2-D), three-dimensional (3-D), planar and curved. Note that a wedge supported by two intersecting discontinuities is a typical 3-D problem with a pre-known hinge-like slip surface. It means that Pan's ''Principle of Maximum'' can be applied directly to the wedge problem rather than using Pan's ''Principle of Minimum'', and only the maximum resistance against potential failure should be determined.

Following the force equilibrium analysis in Section 2, the forces on the plane that is perpendicular to the line of intersection of planes A and B are in equilibrium regardless of what decomposition of force $\boldsymbol{T_{rn}}$ is used. Only force $\boldsymbol{T_{rs}}$ leads to a potential failure along the line of intersection, hence, a resistance contributed by shear forces $\boldsymbol{S}_{11}$ and $\boldsymbol{S}_{22}$ should be mobilized against the potential failure (Fig. 2c). Eqs. (8) and (9) show that $\boldsymbol{S}_{11}$ and $\boldsymbol{S}_{22}$ are related to force $\boldsymbol{T_{rn}}$ by the two angles θ_1 and θ_2.

An optimization method can be applied to search for the maximum resistance of $\boldsymbol{S}_{11}+\boldsymbol{S}_{22}$ against force $\boldsymbol{T_{rn}}$ that leads to a potential failure among all possible combinations of θ_1 and θ_2. It should be mentioned herein that c_e and ϕ_e are replaced by c and ϕ when calculating the magnitude of $\boldsymbol{S}_{11}+\boldsymbol{S}_{22}$. Once the maximum resistance $\boldsymbol{S}_{11}+\boldsymbol{S}_{22}$ has been obtained, θ_1, θ_2, β_1 and β_2 are determined accordingly (Fig. 2c). The factor of safety F can be obtained by using Eq. (11).

In the process of searching for the maximum mobilized resistance $\boldsymbol{S}_{11}+\boldsymbol{S}_{22}$, combinations of θ_1 and θ_2 must guarantee not to violate the following physical conditions

$$R_{1s} \leqslant R_{1n} \cdot \tan\phi_1 + c_1 \cdot A_1, \tag{13}$$

$$R_{2s} \leqslant R_{2n} \cdot \tan\phi_2 + c_2 \cdot A_2. \tag{14}$$

Substitution of Eqs. (3), (5) and (6) into Eq. (13) yields

$$\sin\alpha_1 - \cos\alpha_1 \cdot \tan\phi_1 \frac{c_1 \cdot A_1 \cdot \sin(\theta_1+\theta_2)}{\sin\theta_2 \cdot \sin\alpha \cdot T_r}. \tag{15}$$

Similarly,

$$\sin\alpha_2 - \cos\alpha_2 \cdot \tan\phi_2 \leqslant \frac{c_2 \cdot A_2 \cdot \sin(\theta_1+\theta_2)}{\sin\theta_1 \cdot \sin\alpha \cdot T_r}. \tag{16}$$

In addition, reactions $\boldsymbol{R}_1$ and $\boldsymbol{R}_2$ must be directed upward in order not to violate the condition of force equilibrium (Fig. 2b), that is,

$$0 \leqslant \theta_1, +\theta_2 \leqslant 180^\circ. \tag{17}$$

The method, which uses Pan's ''Principle of Maximum'' and optimization techniques to search for the maximum resistance and the corresponding F based on limit equilibrium approach, is called herein general limit equilibrium (**GLE**) method.

5. Upper Bound (UB) Method

The upper bound theorem of limit analysis in classic plasticity is widely applied in geotechnical engineering due to its simplicity and no need to perform the complicated stress or force analysis (Chen, 1975). The upper bound theorem for slope stability analysis is stated as follows for a kinematically admissible strain rate within a plastic zone Ω^* of a potential sliding mass and a velocity field $\boldsymbol{V}^*$ of the same sliding mass along a slip surface Γ^*, the external surface load $\boldsymbol{T}^*$ calculated from

$$\int_{\Omega^*} \sigma^*{}_{ij}\dot{\varepsilon}^*_{ij} d\Omega^* + \int_{\Gamma^*} \sigma_{\Gamma^*}\dot{\varepsilon}^*_{\Gamma^*} d\Gamma^* = \boldsymbol{G}\boldsymbol{V}^* + \boldsymbol{T}^*\boldsymbol{V}^* \tag{18}$$

will be either greater than or equal to the real surface load $\boldsymbol{T}$. In Eq. (18) the first term is the rate of work done by stress σ^*_{ij} over strain rate $\dot{\varepsilon}^*_{ij}$, dissipated within Ω^*. The second term is the rate of work done by the traction σ_{Γ^*} over Γ^*. The right side terms in Eq. (18) represent the rate of external work done by weight of sliding mass $\boldsymbol{G}$ and the surface load $\boldsymbol{T}^*$ over the velocity field $\boldsymbol{V}^*$ (Donald and Chen, 1997).

It should be mentioned herein that the resultant force $\boldsymbol{P}$ of pore water pressure u applied on discontinuities is considered to be an external force and does not appear in the energy equation in Eq. (18). If there is a pore water pressure, the effective cohesion and friction angle shall be used. To include the pore water pressure force, the energy balance equation is then changed to

$$\int_{\Omega^*} \sigma^*_{ij}\dot{\varepsilon}^*_{ij} d\Omega^* + \int_{\Gamma^*} \sigma_{\Gamma^*}\dot{\varepsilon}^*_{\Gamma^*} d\Gamma^* = \boldsymbol{W}\boldsymbol{V}^* + \boldsymbol{T}^*\boldsymbol{V}^* + \boldsymbol{P}\boldsymbol{V}^*. \tag{19}$$

Note that the wedge body is considered as a potential failure mass while the two discontinuities as the slip surface. The wedge body is generally assumed to move as a rigid body along its two intersecting discontinuities. No internal energy is, therefore, dissipated within the wedge body and the first terms of Eqs. (18) and (19) diminish. If the discontinuities are viewed as a shear band with no thickness, the second terms of Eqs. (18) and (19) can be simplified to the energy dissipation $\dot{\boldsymbol{D}}$ along a shear band (Fig. 3). By applying the associated flow rule and the Mohr-Coulomb failure criterion, $\dot{\boldsymbol{D}}$ along a shear band with unit length per volume is defined as (Chen, 1975)

$$\dot{\boldsymbol{D}} = c \cdot \cos\phi \cdot V \tag{20}$$

where c and ϕ are cohesion and friction angle associated with the shear band, V is a velocity jump inclined of ϕ with respect to the shear surface (Fig. 3).

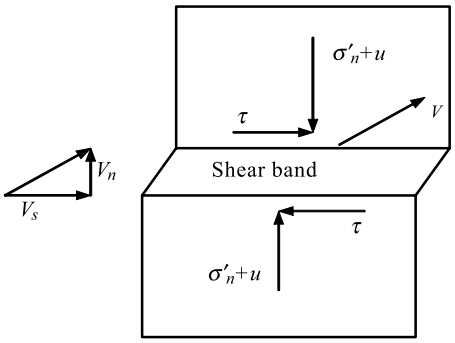

Fig. 3. A mode of shear deformation in a shear band

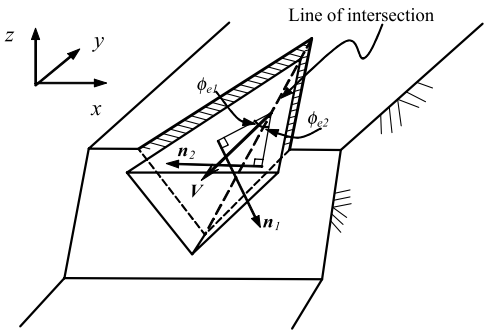

Fig. 4. An schematic illustration of the movement of a wedge

For stability analysis of a slope containing a wedge resting on two interesting discontinuities, the application of the upper bound theorem involves two steps:

Step 1: Determining the velocity of wedge.

Figure 4 illustrates a typical movement of a wedge with a velocity $\boldsymbol{V}$, inclining at a mobilized friction angle ϕ_{e1} with respect to plane A and at a mobilized friction angle ϕ_{e2} to plane B. The components of the velocity $\boldsymbol{V}$ in the (x, y, z) coordinate system are denoted by $(v_x, v_y\ v_z)$. Similarly, the unit vector $\boldsymbol{n}_1$ normal to plane A is denoted by (n_{1x}, n_{1y}, n_{1z}) while the unit vector $\boldsymbol{n}_2$ normal to plane B is denoted by (n_{2x}, n_{2y}, n_{2z}). The fact that the wedge velocity $\boldsymbol{V}$ inclines at an angle ϕ_{e1} to plane A indicates that the angle between $\boldsymbol{V}$ and $\boldsymbol{n}_1$ will be $\pi/2 - \phi_{e1}$, which yields

$$\Phi(\boldsymbol{V} \bullet \boldsymbol{n}_1) = \cos(\pi/2 - \phi_{e1}) = \sin\phi_{e1}. \tag{21}$$

Similarly

$$\Phi(\boldsymbol{V} \bullet \boldsymbol{n}_2) = \cos(\pi/2 - \phi_{e2}) = \sin\phi_{e2}, \tag{22}$$

where $\Phi(\boldsymbol{V} \bullet \boldsymbol{n_i})$ is the scalar product of vectors $\boldsymbol{V}$ and $\boldsymbol{n_i}$ and is determined by

$$\Phi(\boldsymbol{V} \bullet \boldsymbol{n_i}) = \frac{v_x \cdot n_{ix} + v_y \cdot n_{iy} + v_z \cdot n_{iz}}{\sqrt{v_x^2 + v_y^2 + v_z^2} + \sqrt{n_{ix}^2 + n_{iy}^2 + n_{iz}^2}} (i = 1, 2). \tag{23}$$

Note that since only two equations (Eqs. (21) and (22)) are available for the three unknown components (v_x, v_y, v_z) of $\boldsymbol{V}$, one additional equation must be introduced. In addition, considering that it has no influence on the construction of energy balance equation and the solution for the factor of safety, the magnitude of $\boldsymbol{V}$ is generally assumed to be unity

$$|\boldsymbol{V}| = \sqrt{v_x^2 + v_y^2 + v_z^2} = 1. \tag{24}$$

Thus, the three unknown components v_x, v_y and v_z can be determined by solving a system of non-linear equations (21), (22) and (24) for given values of ϕ_{e1} and ϕ_{e2}.There are two sets of v_x, v_y and v_z that can be obtained due to Eq. (24). The right one should be able to guarantee that the potential sliding of wedge is downward and outward rather than upward and inward relative to readers (Fig. 4).

Step 2: Establishing the energy balance equation and finding the factor of safety.

The external forces acting on the wedge, which do the external work rate, include weight of the wedge $\boldsymbol{G}$, surface resultant force $\boldsymbol{T}$ and water force $\boldsymbol{P}_1$ and $\boldsymbol{P}_2$ acting on planes A and B (Fig. 1). Thus, the work rate in the direction of velocity V done by the above forces can be expressed as a sum of their scalar products

$$W = |\boldsymbol{G}| \cdot |\boldsymbol{V}| + |\boldsymbol{T}| \cdot |\boldsymbol{V}| + |\boldsymbol{P}_1| \cdot |\boldsymbol{V}| + |\boldsymbol{P}_2| \cdot |\boldsymbol{V}| \tag{25}$$

The total energy dissipated on the discontinuities (planes A and B) due to $\boldsymbol{V}$ is

$$\sum \dot{\boldsymbol{D}} = c_{e1} \cdot A_1 \cdot |\boldsymbol{V}| \cdot \cos \phi_{e1} + c_{e2} \cdot A_2 \cdot |\boldsymbol{V}| \cdot \cos \phi_{e2}. \tag{26}$$

The factor of safety F, included in the mobilized cohesion and friction angle in Eq. (26), can be determined by equating the work rate done by external forces (Eq. 25) to the total energy dissipation on discontinuities (Eq. 26)

$$\begin{aligned} &c_{e1} \cdot A_1 \cdot |\boldsymbol{V}| \cdot \cos \phi_{e1} + c_{e2} \cdot A_2 \cdot |\boldsymbol{V}| \cdot \cos \phi_{e2} \\ &\quad = |\boldsymbol{G}| \cdot |\boldsymbol{V}| + |\boldsymbol{T}| \cdot |\boldsymbol{V}| + |\boldsymbol{P}_1| \cdot |\boldsymbol{V}| + |\boldsymbol{P}_2| \cdot |\boldsymbol{V}| \end{aligned} \tag{27}$$

Note that the factor of safety F involved in Eq. (27) should be determined by using an iterative procedure (Donald and Chen, 1997). Once F has been determined, the direction of $\boldsymbol{V}$ is known according to the mobilized strength parameters. The directions of shear forces acting on planes A and B are in the projections of $\boldsymbol{V}$ on these two planes respectively, but opposite to these projections. Then, the angle β between the shear forces acting on planes A and B and their line of intersection can be determined following the procedure presented for the GLE method. In addition, application of the upper bound theorem indicates that the solution obtained by the above procedure is an upper bound, or in other words, a solution that offers the maximum resistance.

6. Comparison of TLE, GLE, UB and DD Methods

Two rock wedge example problems are analyzed by using the TLE, GLE, UB methods and the method which account for the dilatancy of discontinuous planes (called DD method in this paper) proposed by Wang and Yin (2002). The values of the factor of safety obtained by using the four methods are compared. The relationships and differences of the four methods are explored.

Example 1: The first example is a symmetrical rock wedge (Wang and Yin, 2002). Plane A dips at 60° in a dip direction of 120° while plane B dips at 60° in a dip direction of 240°. The wedge is 10.2 m high. Strength parameters on plane A are the same as those on plane B. Herein, two sets of strength parameters are used. One is $c = 10$ kPa and $\phi = 30°$, while the other $c = 0$ kPa and $\phi = 30°$. Note that for this specific example, the weight $\boldsymbol{G}$ is the only external load applied to the wedge. Strength parameters and geometry conditions are symmetrical about the vertical plane passing the line of intersection of planes A and B, therefore, shear forces on planes A and B should incline at the same angle β to the line of intersection.

Values of the factor of safety F and angle β for the two sets of strength parameters determined by the TLE, GLE, UB and DD methods are given in Table 1. Variations of the factor of safety determined by the TLE, GLE and UB methods with cohesion and friction angle are also presented in Fig. 5.

Table 1. Values of F and β obtained by the TLE, GLE, UB and DD methods for Example 1

Method	$c = 0$ kPa, $\phi = 30°$		$c = 10$ kPa, $\phi = 30°$	
	F	β (°)	F	β (°)
TLE	0.869	0.0	1.228	0.0
GLE	1.136	40.2	1.430	30.7
UB	1.136	–	1.430	–
DD($\psi_e = 0$)	0.869	0.0	1.228	0.0
DD($\psi_e = \phi_e$)	1.136	40.2	1.430	30.7

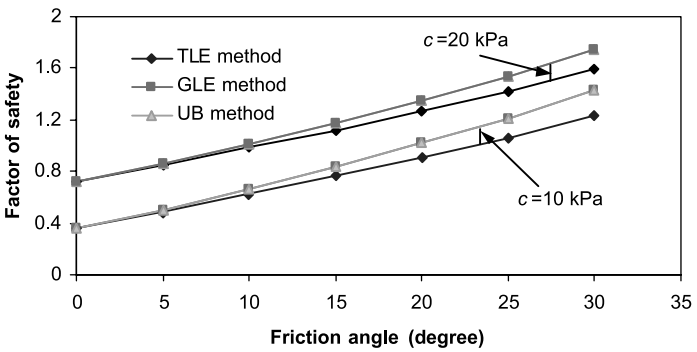

Fig. 5. Variations of the factor of safety determined by the TLE, GLE and UB methods with cohesion and friction angle

Table 2. Values of F and β obtained by TLE, GLE, UB and DD methods for Example 2

Method	Factor of safety F	β_1 (°)	β_2 (°)
TLE	1.846	0.0	0.0
GLE	1.929	19.5	14.7
UB	1.929	–	–
DD($\psi = 0$)	1.846	0.0	0.0
DD($\psi = \phi_e$)	1.929	19.4	14.7

Table 1 and Fig. 5 show that both the TLE method and DD method with zero dilation angle give the same minimum value of the factor of safety while the GLE method, UB method and DD method with the maximum mobilized dilation coefficient give the maximum value of the factor of safety. Furthermore, shear forces on slip surfaces determined by the GLE and UB methods incline at a certain angle to the line of intersection of planes A and B. Figure 5 also shows that when the friction angle is zero, all methods give the same value of the factor of safety for the same value of cohesion. For a given value of cohesion, however, the difference in the values of the factor of safety determined by the TLE and GLE (and UB or DD) methods increases with the friction angle. When the friction angle reaches the maximum of 30° in this study, the difference in the factor of safety reaches the maximum, and the relative difference is up to 22%.

Example 2: The second example is a non-symmetrical wedge problem that is frequently quoted in the literature (Hoek and Bray, 1977). The geometry and material properties for this example are reported in Wang and Yin (2002).

Values of the factor of safety and angles between shear forces on slip surfaces and the line of intersection of planes A and B determined by the TLE, GLE, UB and DD methods are summarized in Table 2. Since the TLE method assumes that shear forces on planes A and B incline at an angle of zero to the line of intersection of planes A and B, the minimum value of the factor of safety, 1.846, is obtained. The GLE method, however, presents the maximum value of the factor of safety, 1.929, while the shear forces on planes A and B incline at 19.4° and 14.7° to the line of intersection, respectively. The UB method gives the same value of factor of safety as the GLE method. When varying the dilatancy properties of planes A and B, the DD method gives the same minimum value as the TLE method at zero dilatancy angle, and the same maximum value of factor of safety and β_1, β_2 as that obtained by using the GLE and UB methods at the full dilatancy angles.

7. Finite Element Analysis

To further investigate the influence of the direction of shear forces acting on two intersecting discontinuities on the factor of safety, three-dimensional (3-D) finite-element (FE) analyses for the two examples discussed in Section 6 are performed by using the commercial code ABAQUS (1995). In the 3-D FE analysis, the wedge is modeled into three parts: a wedge body that rests on two intersecting discontinuities, a zone of discontinuity that consists of the two interesting discontinuities and a wedge base (or rock body) below the discontinuity zone.

The wedge body is discretized into a number of layers of three-dimensional (3-D) solid elements which exhibit a linearly elastic isotropic behaviour. The discontinuous zone is simulated by two layers of 3-D solid elements that are plate-like and follow the linear Drucker-Prager failure criterion. The wedge base underneath the discontinuity zone is simulated by fixed supports.

Based on the preceding understanding of the wedge problem, a potential sliding will occur along the two discontinuities (discontinuities have lower strength than a wedge body and a wedge base). The 3-D FE analysis of the wedge problem focuses on investigating the state of stress and deformation characteristics of the discontinuity zone. An external load (gravity or a surface load) is gradually applied through the 3-D solid elements of the wedge. The total reactions of fixed supports to the discontinuity zone (slip surface) associated with a set of cohesion and friction angle of the discontinuity zone can be obtained when the stress state of the discontinuity zone reaches a Mohr-Coulomb state or a fully plastic state (the detailed procedures will be presented in the following). Determination of the factor of safety is transferred to obtain a set of mobilized cohesion and friction angle values that make the state of stress in the discontinuity zone in a Mohr-Coulomb state.

7.1 Finite Element Analysis of Example 1

7.1.1 3-D FE Modelling

Since the geometry and strength parameters of the wedge in example 1 are symmetrical, only the right-hand half of the wedge (tetrahedron DABC as shown in Fig. 6a) is taken and analyzed. A 3-D finite element model for the symmetrical problem is explained in details as follows:

a) To easily discretize the tetrahedron DABC into 3-D solid elements and to number nodes and elements, a very small part of tetrahedron $DA_1B_1C_1$ (for clarity, sides DA_1, DB_1, and DC_1 which have been enlarged in Fig. 6a) is removed. The sides DA_1, DB_1, and DC_1 are generally taken as $1/100$ of the length of the sides DA,

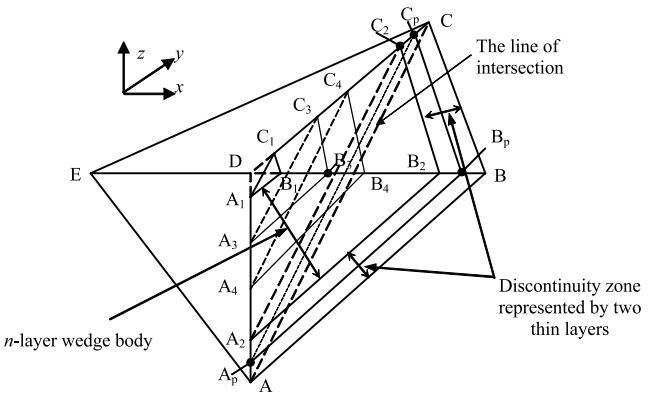

Fig. 6a. Schematic discretization of the symmetrical wedge in Example 1

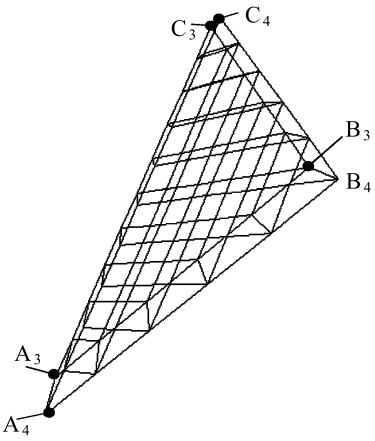

Fig. 6b. Illustration of elements in one layer

DB, and DC, respectively. Therefore, the removal of tetrahedron $DA_1B_1C_1$ has no significant influence on the FE results.

b) The discontinuity zone is generally thin and is represented by prism $A_2B_2C_2$–ABC. The length of AA_2, BB_2, and CC_2 are taken to be $1/100$ of sides DA, DB, and DC, respectively. Prism $A_2B_2C_2$–ABC for the discontinuty zone is divided into two layers (the two-layer discretization being fixed in this study) by a middle plane $A_pB_pC_p$ that is formed by connecting the midpoints of the sides AA_2, BB_2 and CC_2.

c) The wedge body, which is represented by prism $A_1B_1C_1$–$A_2B_2C_2$, is divided into n-layers of prisms by n-1 planes (e.g. planes $A_3B_3C_3$ and $A_4B_4C_4$). The number n is determined by a study of the mesh convergence. Every layer (e.g. prism $A_3B_3C_3$–$A_4B_4C_4$) is further discretized into a series of 3-D 6-node linear triangular prisms and 8-node linear brick elements as shown in Fig. 6b.

d) The number of nodes and elements composing each layer for the wedge body and the discontinuity zone are the same. The only difference is the dimension of elements. The wedge base is simulated by fixed supports to the bottom side of the slip zone.

It should be mentioned that the nodes in the symmetrical plane C_1CAA_1 (in y–z plane) are fixed in the x-direction, but free to move in the y–z plane. The nodes on the bottom of the wedge body mesh are connected to the nodes of the top layer of the discontinuity zone in plane $A_2B_2C_2$.

7.1.2 A Study of the Mesh Convergence

For the symmetrical wedge problem shown in Fig. 6a, two different discretization models of prism $A_1B_1C_1$–$A_2B_2C_2$ into 9-layers (coarse) and 14-layers (fine) with a different number of elements for each layer are studied and compared.

An isotropic linear elastic model with Young's modulus $E_{\text{wedge}} = 25\,\text{MPa}$, and Poisson's ratio $\nu_{\text{wedge}} = 0.17$ is used to model the wedge material. A linear Drucker-

Prager elasto-plastic model with cohesion $c = 10\,\text{kPa}$ and a friction angle $\phi = 30^\circ$ is used to model the slip zone. For the elastic properties the following is assumed: $E_{\text{slip}} = 10\,\text{MPa}$, and $\nu_{\text{slip}} = 0.15$. In the mesh convergence study for the symmetrical wedge problem, only the associated flow rule is considered. The unit weights of the materials for the wedge body and the slip zone are the same, that is, $\gamma_{\text{wedge}} = \gamma_{\text{slip}} = 26.46\,\text{kN/m}^3$.

When the gravity of the wedge is gradually applied to the three-dimensional finite element mesh, reactions of all nodes on plane ABC are obtained by using finite element analysis. The resultant reaction $\boldsymbol{R}$ of all nodes on the plane ABC of the slip zone supporting the wedge is a sum of reactions of each node on plane ABC, and is given by

$$\boldsymbol{R} = [R_x, R_y, R_z]^{\text{T}}, \tag{28}$$

where

$$R_x = \sum_{i=1}^{n} r_{xi};\ R_y = \sum_{i=1}^{n} r_{yi};\ R_z = \sum_{i=1}^{n} r_{zi}, \tag{29}$$

where r_{xi}, r_{yi}, and r_{zi} are the components of reaction of node i in x, y and z directions. n is the number of nodes on plane ABC.

Table 3 summarizes the components of reaction $\boldsymbol{R}_2$ in x, y and z directions for different discretization models. Columns 2 and 3 in Table 3 are the number of layers representing the wedge and number of nodes on each plane, respectively. Column 4 is the number of all elements in the 3-D FE model. Columns 5, 6, and 7 are the components of total reaction $\boldsymbol{R}$ in x, y and z directions.

Since the wedge problem is symmetrical in geometry and loading, the magnitude of the reaction $\boldsymbol{R}$ in z-direction (opposite to the gravity) should be equal to 2350.2 kN, i.e., half weight of the wedge. This is demonstrated by the values shown in column 7, Table 3. In addition, since the wedge is symmetrical about plane C_1CAA_1 as shown in Fig. 6a, R_y is zero as given in column 6, Table 3.

Variations of R_x with different 3-D FE meshes show that the number of layers in the wedge body has little influence on the magnitude of R_x. However, the magnitude of R_x considerably depends on the number of nodes in each plane. It is found from Table 1 that the discretization model No. 9 with 9 layers and 676 nodes in each plane gives a

Table 3. Values of R_x, R_y and R_z for different 3-D discretization models for Example 1 ($c = 10\,\text{kPa}$, $\phi = 30^\circ$)

Model no.	Number of layers	Number of node on one plane	Number of total elements	R_x (kN)	R_y (kN)	R_z (kN)
1	9	36	270	−1471.43	0.0	2350.1
2	9	64	504	−1475.47	0.0	2350.2
3	9	121	990	−1480.02	0.0	2350.2
4	9	169	1404	−1482.08	0.0	2350.2
5	9	256	2160	−1484.48	0.0	2350.2
6	9	400	3420	−1486.82	0.0	2350.2
7	14	400	5320	−1490.48	0.0	2350.2
8	19	400	7220	−1490.71	0.0	2350.2
9	**9**	**676**	**5850**	**−1492.09**	**0.0**	**2350.2**
10	14	676	9110	−1492.77	0.0	2350.2

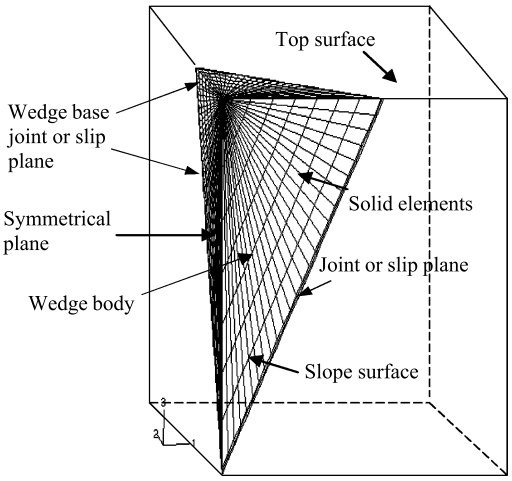

Fig. 7. Undeformed 3-D FE mesh for the symmetrical wedge in Example

reasonably accurate value of $R_x = -1492.09\,\text{kN}$. Therefore, a discretization with 9 layers and 676 nodes is utilized in the following FE analyses of this symmetrical wedge problem. Figure 7 shows an undeformed 3-D finite element mesh for the right-hand half of this symmetrical example.

7.1.3 Determination of the Factor of Safety

In this study, a linear Drucker-Prager elasto-plastic model is used as an approximation to the Mohr-Coulomb model. For a set of values of cohesion and friction angle, the state of stress on the slip surface (the discontinuity zone) is likely to be fully elastic, fully plastic, partially elastic and plastic, or no existing. Therefore, whether or not the state of stress on the slip surface reaches the Mohr-Coulomb failure state is dependent upon the combination of cohesion and friction angle associated with these slip surfaces when external loadings are given.

When a set of cohesion and friction angle values is specified to perform 3-D FE analysis, a state of stress on discontinuity zone can be obtained. If the tangential and normal components of $\boldsymbol{R}$ satisfy the Mohr-Coulomb failure criterion, the state of stress is considered to be in a Mohr-Coulomb state and the set of cohesion and friction angle values are referred to as a set of Mohr-Coulomb-state cohesion and friction angle values accordingly. Note that the Mohr-Coulomb-state cohesion and friction angle values will not be reduced by the factor of safety, therefore, a Mohr-Coulomb state is also called the state for $F = 1$.

For the symmetrical problem in Fig. 6a when the reaction $\boldsymbol{R}$ of plane ABC (a slip plane) is decomposed into its normal and tangential components $\boldsymbol{R_n}$ and $\boldsymbol{S}$, a yielding coefficient is defined as

$$\kappa = \frac{|\boldsymbol{R_n}|\tan\phi + cA}{|\boldsymbol{S}|}, \tag{30}$$

where c and ϕ are the cohesion and the friction angle associated with the Mohr-Coulomb failure criterion. A is the area of the slip surface. For the yielding ratio $\kappa = 1$, the stresses computed on the slip surfaces are in a Mohr-Coulomb failure state. The case $\kappa > 1$ means that the state of stress on the slip surfaces has not reached the Mohr-Coulomb failure state. If $\kappa < 1$, the state of stress is beyond the Mohr-Coulomb failure state.

In FE analyses of the wedge problem, the factor of safety F is still defined as $F = \frac{\tan\phi}{\tan\phi_e} = \frac{c}{c_e}$; therefore, mobilized cohesion and friction angle c_e and ϕ_e that involve the factor of safety are input into Eq. (30) to compute the yielding ratio κ. Since it is difficult to directly determine which set of mobilized cohesion and friction angle that make $\kappa = 1$, the factor of safety needs to be determined by a trial-and-error procedure, as follows:

(a) to choose an initial estimate of F that is less than that obtained by the TLE method;
(b) to calculate values of $c_e = \frac{c}{F}$ and $\phi_e = \tan^{-1}(\frac{\tan\phi}{F})$. An FE analysis is followed to determine values of R_z and κ;
(c) to stop the FE analysis when R_z is less than half weight of the wedge (2350.2 KN) or $\kappa < 1$; otherwise, to gradually increase the value of the factor of safety and go to Step (b);
(d) to plot the variation of κ with F, and to find the value of F at $\kappa = 1$.

For $c = 10$ kPa and $\phi = 30°$, a plot of κ versus F shows that the factor of safety decreases with the yielding coefficient (Fig. 8). When the value of κ is 1.0, the factor of safety F is 1.43, while the tangential component $\boldsymbol{S}$ (shear force on the slip surface) inclines at an angle of 29.9° with respect to the line of intersection of the two interesting discontinuities (Table 4).

7.1.4 Comparison of FE Method with TLE and GLE Methods

As previously discussed, a comparison of the TLE, GLE, UB and DD methods shows that: (a) both the TLE and DD methods for $\psi = 0$ (or zero dilation angle) (Wang and Yin, 2002) give the same minimum factor of safety; (b) the GLE, UB and DD methods

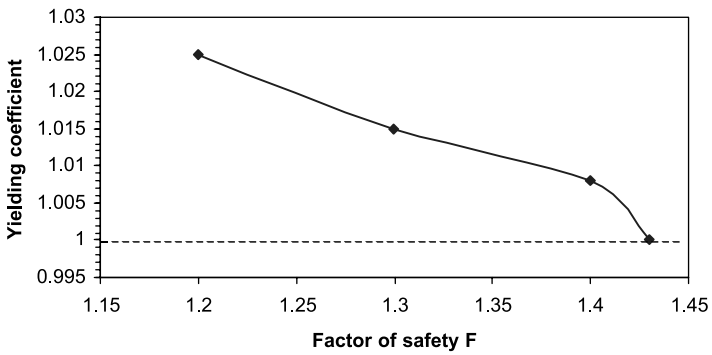

Fig. 8. Variation of the factor of safety with yielding coefficient

Table 4. Values of R_x, R_y, R_z, $|\boldsymbol{R_n}|$, κ and β for different values of factor of safety for Example 1 ($c = 10$ kPa, $\phi = 30°$)

F	R_x (kN)	R_y (kN)	R_z (kN)	$\lvert\boldsymbol{R_n}\rvert$ (kN)	$\lvert\boldsymbol{R_s}\rvert$ (kN)	κ	β (°)
1.2	−2040.0	0.0	2350.2	2594.326	1718.87	1.025	0.2
1.3	−2430.0	0.0	2350.2	2900.4	1736.6	1.015	8.2
1.4	−3092.02	0.0	2350.2	3420.0	1840.6	1.006	20.9
1.5	−2880.05	0.0	1926.0	–	–	–	–
1.45	−2821.33	0.0	2090.2	–	–	–	–
1.44	−3488.77	0.0	2283.6	–	–	–	–
1.43	−3573.85	0.0	2350.2	3798.2	1967.2	1.000	29.9

for $\psi = \phi$ (or for a full dilation angle) (Wang and Yin, 2002) give nearly the same maximum value of the factor of safety. Therefore, only a comparison of the 3-D FE method with the TLE and GLE methods for this symmetrical problem is presented here.

Consistent with the definition in 3-D FE analysis, the Mohr-Coulomb-state cohesion and friction angle are also defined for the TLE and GLE methods. The Mohr-Coulomb-state cohesion and friction angle for the TLE and GLE methods are the cohesion and friction angle that are not altered by the factor of safety (that is, using $F = 1.0$) and make the stress state in the discontinuity zone in a fully plastic state (limit state). A comparison of the Mohr-Coulomb-state friction angle and cohesion determined by the TLE, GLE and FE methods shows that values of the Mohr-Coulomb-state friction angle and cohesion obtained by using the FE method are basically identical to those given by the GLE method (Fig. 9 and Table 5). However, values of the Mohr-Coulomb-state cohesion and friction angle obtained by using the TLE method are greater than those given by the FE or GLE method. Figure 9 also shows that for the same value of cohesion, the TLE method needs a larger friction angle for the wedge to be stable (or for arriving at the Mohr-Coulomb failure state) than friction angles using the FE and GLE methods.

To further explore the difference in the Mohr-Coulomb failure state determined by the TLE, GLE, and FE methods, the magnitudes of $\boldsymbol{R_n}$ and $\boldsymbol{S}$ and the angle β between the direction of $\boldsymbol{S}$ (shear force) and the line of intersection for the three methods are

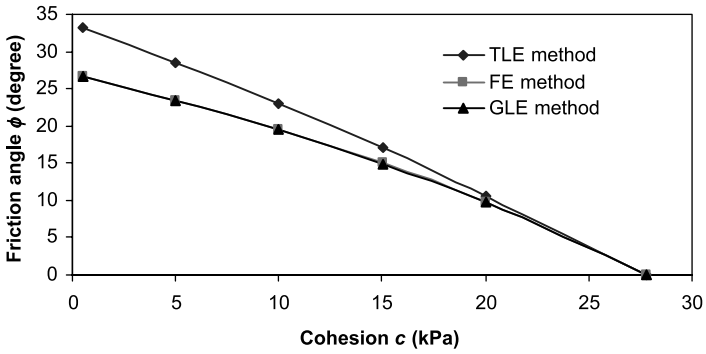

Fig. 9. Values of Mohr-Coulomb-state cohesion and friction angles determined by the TLE, GLE and FE methods

Table 5. Mohr-Coulomb-state cohesions and friction angles determined by the TLE, FE and GLE methods

Cohesion c (kPa)	Friction angle ϕ (°)		
	TLE method	FE method	GLE method
0.5	33.13	26.7	26.64
5	28.59	23.5	23.50
10	23.05	19.56	19.54
15	17.02	15.0	14.95
20	10.57	9.7	9.69
27.82	0.0	0.0	0.0

Table 6. The normal and tangential components of reaction of the discontinuity zone for Example 1

c (kPa)	TLE method			FE method			GLE method		
	$\lvert\boldsymbol{R_n}\rvert$ (kN)	$\lvert\boldsymbol{R_s}\rvert$ (kN)	β(°)	$\lvert\boldsymbol{R_n}\rvert$ (kN)	$\lvert\boldsymbol{R_s}\rvert$ (kN)	β(°)	$\lvert\boldsymbol{R_n}\rvert$ (kN)	$\lvert\boldsymbol{R_s}\rvert$ (kN)	β(°)
0.5	2586.7	1718.8	0.0	4301.6	2119.3	37.6	4375.6	2225.0	39.4
5	2586.7	1718.8	0.0	3941.7	2024.7	31.9	4022.0	2059.0	33.4
10	2586.7	1718.8	0.0	3584.4	1890.0	24.6	3683	1925.0	26.7
15	2586.7	1718.8	0.0	3275.4	1802.9	17.6	3369.0	1827.0	19.7
20	2586.7	1718.8	0.0	2982.0	1747.0	10.3	3068.0	1760.2	12.5
27.82	2586.7	1718.8	0.0	2544.9	1719.2	1.0	2586.0	1719.2	0.0

compared (Table 6). For clarification, only the value of Mohr-Coulomb-state cohesion is listed in Table 6, whereas the value of the corresponding Mohr-Coulomb-state friction angle is reported in Table 5. It can be shown from Table 6 that for any combination of cohesion and friction angle the TLE method gives the same value of $\boldsymbol{R_n}$ and $\boldsymbol{S}$ and that the shear force $\boldsymbol{S}$ inclines at a zero angle to the line of intersection. Both the FE and GLE methods give magnitudes of $\boldsymbol{R_n}$ and $\boldsymbol{S}$ that are greater than those determined by the TLE method. The shear force acting on the slip surface also inclines at angle β greater than zero to the line of intersection. Values of $\boldsymbol{R_n}$ and $\boldsymbol{S}$ and β determined by the FE method are almost the same as those determined by the GLE method.

As discussed above, the TLE method implies that the dilation angle is zero. But the FE method in the paper uses the associated flow rule with a dilation angle ψ equal to the friction angle ϕ. The GLE, UB and DD methods (for $\psi_e = \phi_e$) (Wang and Yin, 2002) all imply the use of a full dilation angle $\psi_e = \phi_e$. With this background, it is easier to understand the differences between the results obtained by using the TLE method and those obtained by using both the FE and GLE methods as shown in Tables 5 and 6. For the same value of cohesion, the FE and GLE methods, which apply the associated flow rule, give lower values of Mohr-Coulomb-state friction angle than the TLE method with zero dilation angle (Table 5), since the dilatancy of discontinuities has been mobilized for resisting the potential failure.

Except for the comparison of Mohr-Coulomb-state cohesion and friction angle, the factor of safety of the symmetric wedge was calculated by using the TLE, GLE, and FE methods for the same cohesion $c = 10$ kPa and different values of friction angle ($\phi = 0$, 10°, 20°, and 30° respectively) (Table 7). The FE method gives basically the

Table 7. Values of the factor of safety determined by the TLE, GLE and FE methods for Example 1

$c = 10$ kPa	ϕ (°)	Factor of safety F		
		TLE method	GLE method	FE method ($\phi = \psi$)
	0	0.360	0.360	0.360
	10	0.625	0.664	0.660
	20	0.907	1.017	1.010
	30	1.229	1.430	1.430

same value of the factor of safety as the GLE method. However, factors of safety determined by the FE and GLE methods are greater than those obtained by the TLE method. When $\phi = 0$, the three methods present the same value of the factor of safety for any value of cohesion.

7.2 Finite Element Analysis of Example 2

7.2.1 3-D FE Modelling

The Example 2 of a non-symmetrical wedge problem was also re-analyzed by using FE modelling. As for the symmetrical wedge problem, a three-dimensional finite element model (see Fig. 10) was set up as follows:

a) The 3-D FE model includes a wedge body (tetrahedron $A_2B_2C_2E_2$) and a discontinuity zone (prisms $A_2B_2C_2$–ABC and $A_2C_2E_2$–ACE). The wedge is split by plane DAC. A very small tetrahedron $A_1B_1C_1E_1$ is cut off for easy FE mesh generation.

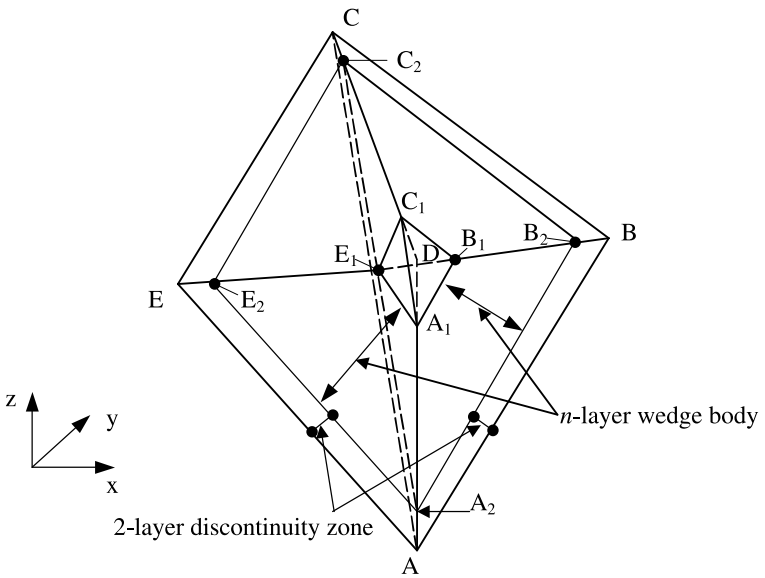

Fig. 10. Schematic discretization of the non-symmetrical wedge in Example 2

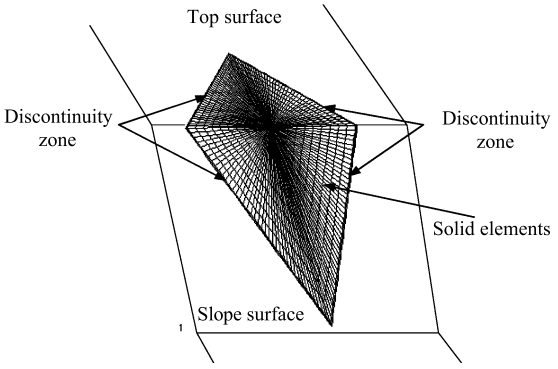

Fig. 11. Undeformed 3-D FE mesh for the non-symmetrical wedge in Example 2

The lengths of sides DA_1, DB_1, DC_1, and DE_1 are taken to be $1/100$ of lengths of sides DA, DB, DC and DE, respectively. It should be noted that point D is at the midpoint of line BE.

b) By using the study of the mesh convergence for the symmetrical wedge problem, prisms $A_1B_1C_1$–$A_2B_2C_2$ and $A_1C_1E_1$–$A_2C_2E_2$, which simulate the wedge body, are respectively divided into 12 layers along the sides A_1A_2, B_1B_2, C_1C_2, E_1E_2 by 11 planes of equal length. Each plane is discretized with 540 nodes. Every layer is further discretized into a series of 3-D 6-node linear triangular prisms and 8-node linear brick elements as shown in Fig. 6b.

The slip zones are represented by very thin plate-like prisms $A_2B_2C_2$–ABC and $A_2C_2E_2$–ACE. Each prism is further divided into two thin layers; each layer is discretized as for the wedge body.

Figure 11 illustrates an undeformed 3-D FE mesh for the non-symmetrical wedge problem. In the FE modeling, the wedge body is considered to be fully elastic and follows the generalized Hooke's Law with modulus of elasticity, $E_{\text{wedge}} = 12\,\text{GPa}$ and Poisson's ratio, $\nu_{\text{wedge}} = 0.17$. The slip zones are simulated by using the linear Drucker-Prager elasto-plastic model. The elastic part of the model is governed by the generalized Hooke's Law with $E_{\text{slip}} = 4.8\,\text{GPa}$ and Poisson's ratio, $\nu_{\text{slip}} = 0.15$. In analysis, the wedge base support (plane ACE – the flatter slip plane and plane ABC – the steeper slip plane) is simplified as fixed nodes. Further, reactions of these fixed nodes are considered to be resultant reactions of the wedge base to the slip surfaces.

7.2.2 Determination of the Factor of Safety F

The non-symmetrical wedge problem involves two slip planes -plane ACD – the flatter slip plane and plane ABC – the steeper slip plane. The fixed node reactions need to be determined. The procedure for determining the factor of safety is similar to that for the symmetrical example. However, the value of the factor of safety that makes both the two yielding ratios associated with the flatter slip plane (κ_1) and steeper slip plane (κ_2) is equal to 1.0. Variations of F with κ_1 and κ_2 (as shown in in Fig. 12) show that κ_1 of

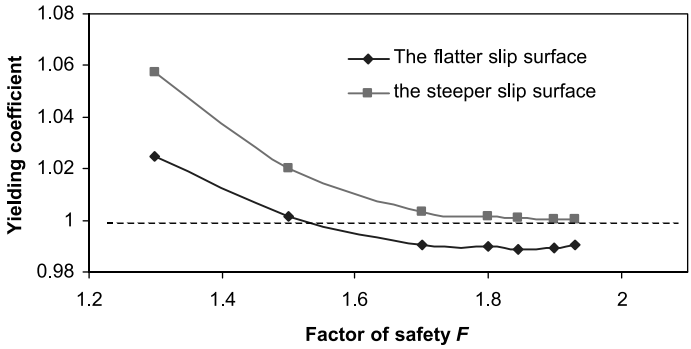

Fig. 12. Variations of yielding coefficient with the factor of safety for the non-symmetrical wedge problem

Table 8. Comparison of analysis results obtained by the TLE, GLE and FE methods for Example 2

Method	F	$\lvert\boldsymbol{R}_{1n}\rvert$ ($\times 10^5$ kN)	$\lvert\boldsymbol{R}_{1s}\rvert$ ($\times 10^5$ kN)	β_1 (°)	$\lvert\boldsymbol{R}_{2n}\rvert$ ($\times 10^5$ kN)	$\lvert\boldsymbol{R}_{2s}\rvert$ ($\times 10^5$ kN)	β_2 (°)
TLE	1.846	1.31	0.37	0.0	0.80	0.46	0.0
GLE	1.929	1.46	0.43	19.4	0.96	0.50	14.7
FE	1.930	1.40	0.38	15.1	0.92	0.49	8.5

the flatter slip surface firstly reaches the Mohr-Coulomb failure state at $F = 1.53$, above which the yielding ratio is maintained at a value of 0.99 (approximately 1.0). The yielding ratio, κ_2, of the steeper slip surface is 1.0 when $F = 1.93$. Theoretically, if the Mohr-Coulomb criterion is used in the finite element analysis, the yielding ratio κ_1 of the flatter slip surface would be 1.0. Since the generalized Drucker-Prager failure criterion is used as an approximation to the Mohr-Coulomb criterion, the value of $\kappa_1 = 0.99$, which is very close to 1.0, is considered to be acceptable.

7.2.3 Comparison of FE Method with TLE and GLE Methods

A comparison of F-values, angles (β_1, β_2), normal forces ($|\boldsymbol{R}_{1n}|$ and $|\boldsymbol{R}_{2n}|$), tangential forces ($|\boldsymbol{S}_1|$and $|\boldsymbol{S}_2|$) obtained by using the FE, TLE and GLE methods (see Table 8) shows that, again for this non-symmetrical example, the TLE method gives the minimum value of factor of safety ($F = 1.846$), and zero angles β_1 and β_2, while the GLE method gives the maximum value of factor of safety ($F = 1.929$), which is about the same as $F = 1.930$ obtained by the FE method with the associated flow rule. The values of β_1 and β_2 determined by the FE method are slightly smaller than those obtained by the GLE method. This means that the shear forces acting on the discontinuity zone are not in the direction of the line of intersection of planes A and B.

7. Conclusions

By exploring ways of determining the direction of the shear force acting on two intersecting discontinuities on which a wedge rests, a general limit equilibrium

method and an upper bound method were derived and presented for stability analysis of the rock wedge problem. These two methods along with the TLE and DD methods were used to analyze two example problems. To further investigate the wedge problem, 3-D FE analyses of the two example problems were also performed and comparisons with the preceding four methods were made.

The solution of the wedge stability problem is dependent on the assumptions regarding the direction of the shear force acting on the two discontinuities. Since the direction of the shear force is assumed to be parallel to the line of intersection of the two discontinuities, the TLE method gives the minimum value of the factor of safety. Since the GLE method searches for the maximum mobilized resistance against failure along the line of intersection and the UB method is based on the associated flow rule, the two methods present the same maximum value of the factor of safety. The two methods indicate that the direction of the shear force inclines at an angle to the line of intersection. This finding is also confirmed by the 3-D FE analyses and the DD method.

The cohesion and friction angle associated with the two discontinuities contribute to the value of the factor of safety differently. For a given value of cohesion, the difference between the minimum value (determined by the TLE method or the DD method for $\psi = 0$) and the maximum value (determined by the GLE method and the FE method) of the factor of safety increases with the friction angle. However, for the same value of friction angle, this difference decreases as the value of cohesion increases. When the friction angle is zero, all the methods presented in this paper give the same value of the factor of safety regardless of the value of cohesion.

Acknowledgements

The research work presented and the preparation of the paper have received financial support respectively from a RGC grant (PolyU 5064/00E) of the University Grants Committee of the Hong Kong Special Administrative Region Government of China, The Hong Kong Polytechnic University, and a grant (No. 59493600) from China National Natural Science Foundation. Their financial support is gratefully acknowledged. The authors wish to thank Mr. Jian CHEN for assistance in the final revision of the paper.

References

ABAQUS (1995): User's Manuals, Version 5.5, Hibbitt, Karlsson & Sorensen, Inc., U.S.A.

Chen, W. F. (1975): Limit analysis and soil plasticity. Elsevier Scientific Publ., New York.

Desai, C. S., Zaman, M. M., Lightner, J. G., Siriwardane, H. J. (1984): Thin-layer element for interfaces and joints. Int. J. Numer. Anal. Methods Geomech. 8, 19–43.

Donald, I., Chen, Z. Y. (1997): Slope stability analysis by the upper bound approach: fundamentals and methods. Can. Geotech. J. 34, 853–862.

Goodman, R. E. (1995): Thirty-fifth Rankine Lecture: Block theory and its application. Geotechnique 45(3), 383–423.

Hoek, E., Bray, J. W. (1977): Rock slope engineering. The Institute of Mining and Metallurgy, New York.

Hoek, E., Bray, J. W., Boyd, J. M. (1973): The stability of a rock slope containing a wedge resting on two intersecting discontinuities. Quart. J. Engng. Geol. 6, 1–55.

Michalowski, R. L. (1995): Slope stability analysis: a kinematical approach. Geotechnique 45, 283–293.

Pan, J. Z. (1980): Stability analysis and landslide assessment for structures. Water Resources Press (in Chinese), Beijing, China.

Wang, Y.-J., Yin, J.-H. (2002): Wedge stability analysis considering dilatancy of discontinuities. Rock Mech. Rock Engng. 35, 127–137.

Authors' address: Prof. Jian-Hua Yin, Department of Civil and Structural Engineering, The Hong Kong Polytechnic University, Hung Hom, Kowloon, Hong Kong, P.R. China; e-mail: cejhyin@polyu.edu.hk